Article:
Mayanna, S, Peacock, CL, Schäffner, F et al. (4 more authors) (2015) Biogenic precipitation of manganese oxides and enrichment of heavy metals at acidic soil pH. Chemical Geology, 402. 6 - 17. ISSN 0009-2541

https://doi.org/10.1016/j.chemgeo.2015.02.029

Biogenic precipitation of manganese oxides and enrichment of heavy metals at acidic soil pH

Sathish Mayanna[a], Caroline L. Peacock[b]*, Franziska Schäffner[a], Anja Grawunder[a], Dirk Merten[a], Erika Kothe[c] and Georg Büchel[a]

[a] Institute of Geosciences, Friedrich-Schiller-University, Burgweg 11, 07749, Jena, Germany
[b] University of Leeds, School of Earth and Environment, LS2 9JT, UK
[c] Institute of Microbiology, Friedrich-Schiller-University, Neugasse 25, 07743, Jena, Germany

*Corresponding author at: University of Leeds, School of Earth and Environment, LS2 9JT, UK.
Tel.: +44(0)113 3437877
Email address: C.L.Peacock@leeds.ac.uk (Caroline L. Peacock)

Abstract

Natural Mn oxides are largely biogenic in origin, formed via the microbial oxidation of Mn(II). These minerals are extremely efficient scavengers of heavy metals, yet to date microbial Mn oxide precipitaion and subsequent heavy metal sorption has received little attention in mining-impacted environments, where heavy metal concentrations are elevated but (bio)geochemical conditions are typically unfavourable for both abiotic and biogenic Mn oxide precipitation, featuring acidic pH and low organic carbon contents. Here we investigate the formation of Mn oxide (bio)geochemical barrier layers, and the immobilization of heavy metals in these layers, in soil profiles from a former uranium mining site in Ronneburg, Germany. Detailed soil profiling shows the site has an acidic soil pH that varies from 4.7 to 5.1 and Eh values from 640 to 660 mV. Using synchrotron X-ray diffraction and X-ray absorption spectroscopy, together with scanning electron microscopy and electron microprobe analysis, we find that the dominant Mn oxide present in the Mn oxide layers is a poorly crystalline hexagonal birnessite, akin to synthetic δ-MnO_2, covering and cementing quartz grains. Using phylogenetic analysis based on 16S rDNA, we identify and characterise six strains of manganese oxidising bacteria (MOB) from the acidic Mn oxide layers which we subsequently culture to produce poorly crystalline hexagonal birnessite akin to that found at the study site. Specifically, we identify three Gram-positive spore-forming firmicutes affiliated to Bacillus safensis, Bacillus altitudinis and Brevibacillus reuszer, which are able to oxidize Mn after initiating spore formation, two Gram-positive actinobacteria belonging to the genera Arthrobacter and Frondihabitans, and one Gram-negative proteobacteria belonging to the genus Sphingomonas. Geochemical thermodynamic speciation modeling indicates that the abiotic precipitation of Mn oxides in the Mn oxide layers is unfavourable and we suggest that the Mn oxides in the (bio)geochemical barriers at our study site are biogenically precipitated in an acidic soil environment. To our knowledge, this is the first report to identify the above six bacterial strains, and specfically identify spore-forming bacteria, as MOB in an acidic soil environment. We find that the poorly crystalline hexagonal birnessite precipitated in the Mn oxide layers efficiently immobilises Ba, Ni, Co, Cd, Zn and Ce, and as such we find that MOB and biogenically precipitated Mn oxides can exert a strong control on the fate and mobility of metals in mining-impacted environments.

Keywords: (Bio)geochemical barrier; manganese oxidizing bacteria; birnessite; acidic pH; metal sorption.

1. Introduction

Heavy metals discharged from industrial processes, mining activities and municipal wastes are widespread pollutants of great concern. Despite a requirement for some heavy metals as essential trace elements (bio-essential), heavy metals are toxic to life at elevated concentrations and are non-degradable and thus persistent in the environment (e.g., Bradl, 2004). Their ubiquity and elevated concentrations in waters and soils warrants research into ways to lower ecotoxicity through immobilization, which in oxic environments can be achieved through sorption onto and (co)precipitation with hydrous oxides of Mn and/or Fe (e.g., Fuller and Harvey, 2000; Lee et al., 2002). In particular, heavy metals can be immobilised in oxic environments by so called geochemical barriers of Mn(III/IV) or Fe(III) (hydr)oxides (e.g., Burkhardt et al., 2009; Perel'man, 1986), which in turn aids in the clean-up of heavy metals from contaminated sites (e.g., Peng et al., 2009).

The concept of a geochemical barrier was first introduced by Perel'man in 1961, and later defined as a local epigenetic zone where the conditions governing element migration are drastically altered, resulting in a substantial accumulation of selected elements (Perel'man, 1961; Perel'man, 1967). A variety of barriers can be differentiated (Perel'man, 1986), but common to most barriers developing in oxic environments, such as near-surface environments impacted by mining activities, is the deposition of Mn and Fe (hydr)oxides. In particular, Mn oxides are extremely reactive and amongst the strongest oxidants in the environment, and can therefore instigate coupled sorption and redox reactions over a wide pH range (e.g., Post, 1999). These reactions are known to exert a strong control on the speciation, mobility and bioavailability of many bio-essential and toxic heavy metals, including Ba, Co, Cu, Ni, Ag, Zn, Pb, Tl and Hg (e.g., Manceau et al., 2007; Manceau et al., 1986; Manceau et al., 2003; Nelson et al., 1999; Nelson et al., 2002; Peacock, 2009; Peacock and Moon, 2012; Peacock and Sherman, 2004; Perel'man, 1986; Post, 1999; Sherman and Peacock, 2010), and Mn oxides are able to degrade or oxidize different inorganic and organic compounds, rendering them less toxic, including Cr(III), Co(II) (e.g., Manceau and Charlet, 1992; Takahashi et al., 2007), hydrogen sulphides (e.g., Bargar et al., 2005a), humic and fulvic acids (e.g., Tipping and Heaton, 1983), and aromatic hydrocarbons (e.g., Lehmann et al., 1987).

Mn oxides are formed via the oxidation of dissolved Mn(II). However, in the environment, the chemical oxidation of Mn(II) at acidic pH is thermodynamically unfavourable

and at circumneutral-alkaline pH is slow (e.g., Morgan, 2005). Oxidation of Mn(II) by microorganisms increases the oxidation reaction rate by several orders of magnitude compared to abiotic reactions (e.g., Morgan, 2005; Tebo et al., 2004; Tebo et al., 2007). Accordingly it is widely accepted that natural Mn oxides are largely biogenic in origin, formed via microbial oxidation of Mn(II) (e.g., Anderson et al., 2009; Bargar et al., 2005b; Bargar et al., 2000; Brouwers et al., 2000; Francis and Tebo, 2001; Miyata et al., 2007; Saratovsky et al., 2006; Spiro et al., 2009; Tebo et al., 2004; Tebo et al., 2005; Villalobos et al., 2003; Webb et al., 2005a; Webb et al., 2005b). Abiotic oxidation of Mn(II) at ~ neutral pH typically produces phyllomanganate (layer-type) phases of the birnessite mineral group, with either triclinic or hexagonal symmetry, and with varying degrees of crystallinity, from poorly crystalline δ-MnO_2 to crystalline birnessite (e.g., Villalobos et al., 2003). Biogenic oxidation of Mn(II) at ~ neutral pH, utilizing Mn(II) oxidizing microbes including Pseudomonas putida GB-1 and MnB1 (e.g,, Villalobos et al., 2006; Villalobos et al., 2003; Zhu et al., 2010), Bacillus SG-1 (e.g., Bargar et al., 2005b; Mandernack et al., 1995) and Leptothrix discophora SS-1 (e.g., Nelson et al., 1999), typically produces a phase that is very poorly crystalline but mineralogically and morphologically similar to δ-MnO_2 (e.g., Webb et al., 2005a).

To date, microorganisms are well known to oxidise Mn(II) at ~ neutral pH under oxic and hypoxic conditions (e.g., Anderson et al., 2011; Bargar et al., 2005b; Chapnick et al., 1982; Hosseinkhani and Emtiazi, 2011; Luan et al., 2012; Miller et al., 2012; Nelson et al., 1999; Santelli et al., 2010; 2011; Tebo et al., 2005), but our knowledge of microbial Mn(II) oxidation at acidic pH is very limited. Mn(II) oxidation and precipitation of Mn-rich geochemical barriers in acidic pH environments is important however, because the majority of mining impacted environments are characterised by acidic soil pH. Few experiments on biogenic Mn(II) oxidation and the resulting precipitation of Mn oxides in the laboratory at acidic pH have been reported. Bromfield (1979) studied liquid cultures of a soil Streptomyces sp. which can oxidize Mn(II) at pH 4.5 to 5. Other studies on Mn(II) oxidizing alga, Chlorococcum humicolum (Bromfield, 1976), and Mn(II) oxidizing fungi, Cephalosporium sp. (Ivarson and Heringa, 1972), showed that these organisms could oxidize Mn(II) at pH 4.5. Ivarson and Heringa (1972) characterised their Mn oxide products and reported them to be either Mn_3O_4 (hausmanite) or similar to δ-MnO_2.

To improve our understanding of Mn oxide precipitation and heavy metal immobilisation at acidic pH we have investigated a former uranium mining site, located in Ronneburg, Germany, with acidic soil pH and several local epigenetic zones consisting of Mn and Fe hydr(oxides), in which the concentrations of heavy metals, including rare earth elements (REE), are significantly elevated compared to the surrounding soil (Burkhardt et al., 2009; Büchel and Merten, 2009; Carlsson and Büchel, 2005). Very recently two Mn oxidizing bacteria (MOB) have been isolated from this site at pH 5.5, Duganella isolate AB_14 and Albidiferax isolate TB-2, where isolate TB-2 may significantly contribute to Mn oxidation in the acidic Mn-rich soil (Akob et al., 2014). In the work reported here, we sought to further deduce the origin of the Mn oxides in the geochemical barriers and to characterize their heavy metal retention properties. Specifically, we have retrieved intact and undisturbed soil profiles from the site and sampled the barrier layers for Mn oxides and Mn(II) oxidizing bacteria (MOB). Barrier Mn oxides are characterized with electron microprobe analysis, scanning electron microscopy (SEM), synchrotron X-ray diffraction (SR-XRD) and X-ray absorption spectroscopy (XAS). We have also measured geochemical conditions and heavy metal concentrations, throughout the soil profiles. In tandem we have performed thermodynamic speciation modelling to determine the geochemical conditions at the site and whether these are conducive to abiotic Mn oxide precipitation. We report our findings here, concluding that the Mn oxides in the barrier layers are biogenically precipitated, in part by spore-forming bacteria, and are capable of immobilizing high concentrations of heavy metals, at acidic pH conditions.

2. Material and methods

2.1 Sampling and physiochemical characterization of soil profiles

The study site “Gessenhalde” is a former uranium mining site located near Ronneburg, Germany (Fig. 1). The site was active between 1946 and 1990 and produced roughly 200Kt of U (Jakubick et al., 1997). For localization of Mn oxide barriers, 1 m deep manual bore holes (Pürckhauer bore) were cored and screened visually for the presence of Mn oxide layers, identified as horizontal bands of dark brown to black colour. Out of 10 different locations, two positions [profile 1 (P1) at 50°51'15.28" N; 12°8'47.65" E and profile 2 (P2) at 50°51'16.61" N; 12°8'50.10” E] displayed obvious dark colored bands and were subsequently selected for detailed

profile digging in August and September, 2011. Approximately 1 m^3 of soil was manually excavated at P1 and P2 down to the groundwater table (1 to 1.1 m from surface). Each profile contained layers of different soil color (Fig. 2), and as such the depth of each layer and soil color (using a Munsell rock-color chart) were recorded.

Soil redox potential (redox electrode, K-Series, Thermo Scientific, Germany) of each soil layer was measured in situ immediately after excavation (n = 1). Soil solutions from the Mn oxide barrier layers were sampled in situ using Rhizon soil moisture samplers (Eijkelkamp, Germany). These solutions were analyzed for fluoride, chloride, sulfate and nitrate using ion chromatography (DX-120, Dionex, USA). The solutions were also analyzed for Li, Na, K, Mg, Ca, Sr, Ba, Al, Si, Mn, Fe, Co, Ni, Cu, Zn and Cd using inductively coupled plasma optical emission spectrometry (ICP-OES; 725 ES, Varian, Germany) and inductively coupled plasma mass spectrometry (ICP-MS; XSeries II, Thermo Fisher Scientific, Germany). Solution measurements were performed in triplicate and averaged; relative standard deviations were all < 4 %.

Approximately 1 kg of soil per layer was collected in polyethylene bags from different layers of P1 and P2 (Fig. 2). The collected soils were air-dried and sieved (≤ 2 mm; nylon sieves, Linker, Germany). Laboratory measurements were performed for soil electrical conductivity (TetraCon 325, WTW, Germany) and pH using 0.01M $CaCl_2$ soil solutions (BlueLine 11 pH, pH320, WTW) (Grawunder et al., 2009). For soil total carbon content, approximately 500 mg of the ground air-dried and sieved samples were filled in tin sample holders and measured (multi NC 2100, Analytic Jena, Germany). Conductivity and pH measurements were performed in duplicate, while total carbon measurements were performed in triplicate, and averaged; standard deviations were calculated from the repeat measurements.

For particle size distribution a proportion of about 3 g of the fraction ≤ 2 mm was mixed with 0.1M $Na_4P_2O_7 \cdot 10H_2O$ dispersing solution and shaken for 12 h for homogenization and deflocculation. Organic matter in the soil samples was removed with 15% H_2O_2 and 10% HCl, and the samples were washed and centrifuged three successive times with deionized water to remove remnants of the acid. Particle size distribution was determined using laser particle size analyzer (Beckman Coulter LS 13 320, USA). Measurements were performed in triplicate, averaged and expressed as percent size fraction of clay, silt, sand and gravel.

2.2 Metal contents and distribution in soil profiles

The sieved samples (≤ 2 mm) from each profile layer were ground with a centrifugal ball mill (Retsch MM400, Germany) to finer than 63 µm. For total digestion, a pressure digestion system (DAS; PicoTrace, Germany) was used. Approximately, 100-150 mg of the ground samples was filled into TFM vessels with strong acid (2 ml HNO_3, 3 ml 40% HF and 3 ml 70% $HClO_4$; Suprapur, Merck). For sequential extractions (Zeien and Brümmer, 1989) the heavy metals, including radionuclides in the solid phase, were partitioned into seven fractions: (F1) mobile, (F2) specifically adsorbed, (F3) bound to Mn oxides, (F4) bound to organic matter, (F5) bound to amorphous Fe oxides, (F6) bound to crystalline Fe oxides and (F7) the residual fraction (Table 1). Solutions obtained by total digestion and sequential extractions were analyzed for Mn, Fe, Ba, Co, Cd, Zn and Ce by ICP-OES and ICP-MS. Measurements were performed in triplicate and averaged; relative standard deviations were all < 4 %.

2.3 Geochemical modeling of soil solutions from Mn oxide barriers

To evaluate the speciation of Mn in solution and to gain information on the saturation state of different abiotic Mn oxides potentially present in the Mn oxide barriers, pH, EC, Eh and the concentrations of Li, Na, K, Mg, Ca, Sr, Ba, Al, Si, Mn, Fe, Co, Ni, Cu, Zn and Cd, Cl^-, F^-, NO_3^- and SO_4^{2-} measured in the soil pore water from the Mn oxide barrier layers (using Rhizon soil moisture samplers, section 2.1) were implemented in PhreeqC Interactive (release 3.0.2.7614, (Parkhurst and Appelo, 2013)) with the minteq.v4 database (Table 2). We considered the formation of birnessite, which represents the most common Mn oxide in soil systems (Post, 1999), and todorokite, which can be formed during diagenetic transformation of birnessite (e.g., Burns and Burns, 1978). Species distribution was calculated based on molalities.

2.4 Mineralogical characterization of Mn minerals in Mn oxide barriers

2.4.1 Electron microprobe analysis and scanning electron microscopy

Thin sections of undisturbed samples from the Mn oxide barrier layers were prepared on glass slides and coated with carbon (MED 010, Balzers Union, Germany). Chemical composition of the minerals present was determined by energy dispersive x-ray spectroscopy (EDX) spot analyses with a Cameca SX50 (Jeol J×A 8Z30; Electron microprobe microanalyzer, Germany) at 20 kV, 40 nA, beam size 5 µm. Each spot was analysed in triplicate and averaged; relative

standard deviations were all < 10 %. Scanning electron microscopy (SEM) was used to obtain high resolution images of the Mn oxides. Thin sections coated with carbon were mounted on the SEM holder and imaged at 20 eV acceleration voltage using the ULTRA Plus field emission SEM, Carl Zeiss, Jena, Germany.

2.4.2 Synchrotron X-ray diffraction and X-ray absorption spectroscopy

Bulk soil samples from the Mn oxide barriers were subject to SR-XRD at Diamond Light Source (DLS), UK, employing $\lambda = 0.826$ Å at 15 keV on the beamline I11 using a multi-analysing crystal-detector. Samples were ground to < 63 µm, loaded into a borosilicate glass capillary holder (0.5 mm Ø) and sealed. The patterns were obtained at room temperature from 0 to 150 °2θ, with a step size of 0.029 °2θ and a collecting time of 1s per step. A 0.1 g bulk soil sample from the Mn oxide barrier from P2 was also subject to Mn K-edge EXAFS (6.539 keV) at DLS on station B18. The sample was prepared as a pressed pellet and mounted between Kapton tape. EXAFS data were collected for 5 scans in transmission mode. ATHENA (Ravel and Newville, 2005) was used to calibrate from monochromator position (millidegrees) to energy (eV) and to average multiple spectra from the sample, and also to perform background subtraction. The EXAFS fingerprint of the sample spectrum was then compared to a library of reference spectra for a variety of different Mn oxides.

2.5 Isolation of Mn(II)-oxidizing bacteria (MOB) from Mn oxide barriers

Soil samples were collected in sterile 50 ml polypropylene tubes from the surface layers and Mn oxide barriers in both profiles. The samples were immediately transferred and processed in the laboratory. Within two to three hours after sampling, two batches of 5 g of soil from each layer were shaken for 1 h with 45 ml of sterile 0.7% NaCl in a 50 ml polypropylene tube and plated (modified K-medium, per litre: 16 g agar, 0.25 g meat extract, 0.6 g yeast extract, 2 g peptone (soya), 7.5 µg vitamin B12 and 2.4 ml trace element solution (per liter: 1.5 g $FeCl_2 \cdot 4H_2O$, 12.8 g $C_6H_9NO_6$, 0.07 g $ZnCl_2$, 0.006 g H_3BO_3, 0.19 g $CoCl_2 \cdot 6H_2O$, 0.0015 g $CuCl_2$, 0.024 g $NiCl_2 \cdot 6H_2O$ and 0.036 g $Na_2MoO_4 \cdot 2H_2O$) pH 6.5) with $MnCl_2 \cdot 4H_2O$ as Mn^{2+} source at 1 mM and 2 mM concentrations. After two to three weeks at 24 ± 2°C, colonies were counted and transferred to fresh medium and strains identified using colony PCR (universal primers, 16S-27F: 5'-AGA GTT TGA TC(AC) TGG CTC AG-3' and 1492r: 5'-TAC GG(CT) TAC CTT GTT ACG ACT T-3'; Eurofins, Germany) in 48 µl master mix (30.3 µl PCR water,

10 µl buffer 5x, 20 pmol primers, 1 U Mango Taq DNA polymerase (Bioline) and 2.5 µl 50 mM $MgCl_2$, 2 µl template. Cycling was performed as follows: initial denaturation at 95°C for 5 min; denaturation at 95°C for 30 s, annealing at 60°C for 45 s, extension at 72°C for 90 s, with 30 cycles; final extension at 72°C for 10 min. The PCR products were sequenced (GATC Biotech, Germany) and compared to NCBI GenBank entries using BioEdit 7.09 and MAFFT 6 alignments and Treefinder Oct 2010 for phylogenetic reconstruction. The sequences of all 16S rDNA genes have been deposited in GenBank under the accession numbers JX999613 through JX999618. Mn oxidation potential was tested using Leucoberbelin Blue at 0.04% (LBB) and colonies that gave a positive result, indicated by dark blue staining, were obtained as pure cultures. All Mn oxidation potential tests were conducted at least in duplicate on separately plated colonies.

In an attempt to produce biogenic Mn oxides at a pH matching that of the field site, bacterial colonies of the pure cultures that tested positive for Mn oxidizing potential were grown in liquid medium with 0.1 to 1 mM Mn^{2+} concentration at pH ~ 4.8. However, after two weeks of incubation with shaking at room temperature, no Mn(II) oxidation was apparent. Similar studies with closely related bacterial strains to those identified here (e.g., Bacillus pumilus, Francis and Tebo, 2002) have also reported a lack of Mn oxidizing activity from purified spores in liquid media. In light of this, colonies were grown on modified K-medium agar plates in the presence of 1 mM Mn. It is very difficult to solidify agar, inoculate with bacteria and subsequently maintain pH at less than pH ~ 6, and thus the pH was ~ 6.5. Manganese concentration was chosen following Bargar et al. (2005b) who report 1 mM Mn as most favourable for optimum precipitation of Mn oxides by bacterial spores. Colonies were also grown in the presence of 2 mM Ni, where, in the soil samples from the Mn oxide barrier layers, Ni showed the highest overall concentration (total digestion) and the highest concentration in the specific Mn oxide fraction (sequential extraction) of all the heavy metals measured. Nickel concentration was chosen based on resistance experiments on the K-medium agar plates, performed here to identify the maximum concentration of Ni to cause minimal inhibition of bacterial growth. After two weeks of growth at room temperature in the dark, bacterial biomass, containing Mn solid product(s), was carefully scraped off the agar and analysed with SR-XRD. Sections of the agar, containing bacterial biomass and intact colonies, were also mounted on object slides and analyzed for Mn and Ni with LA-ICP-MS, using spot sizes from 180 to 250 µm, laser energy of 1.8 to 2 mJ and at 10 laser shots s^{-1}.

3. Results

3.1 Physiochemical parameters measured in soil profiles

Detailed soil profiling was performed for P1 and P2. Visual observation identified a black Mn oxide barrier layer present in both P1 and P2 at 90 cm and 60 cm depth, respectively (Fig. 2). Overall P1 and P2 consisted of nine and six different soil layers, respectively, clearly distinguishable by soil colour, with each profile including a allochthonic layer (10 YR 5/6) and the Mn oxide barrier (10 YR 3/2).

In P1 soil redox potential, electrical conductivity and pH varied from 549 ±10 to 664 ±10 mV, 163 ±2 to 1360 +17 µS cm^{-1} and pH 3.9 +0.1 to 5.6 ±0.1, respectively (Fig. 2, Table 3). In particular, the Mn oxide barrier showed the highest redox potential of 664 ±10 mV and the lowest EC at 658 ±10 µS cm^{-1} compared to the other layers, and an acidic pH of 4.7 ±0.2. In P2, soil redox potentials were lower than those of P1, ranging from 380 ±10 to 639 ±10 mV, while electrical conductivity ranged from 370 ±7 to 1045 ±20 µS cm^{-1} and pH from 4.3 ±0.1 to 5.1 ±0.2 (Fig. 2, Table 3). The values from the Mn oxide barrier in P2 showed again the highest redox potential of 639 ±10 mV and the lowest EC at 370 ±7 µS cm^{-1} compared to the other layers, and a pH of 5.1 ±0.2. Total carbon content of the Mn oxide barriers showed lower values of 0.28 ±0.2 g kg^{-1} for P1 and 0.20 ±0.1 g kg^{-1} for P2 compared to the other layers (Table 3).

Grain size analysis in P1 showed that the top three layers at 10, 30 and 50 cm depth were similar in grain size composition and mainly composed of sand (up to ~60% of the total grain size distribution at 30 cm depth). However, in the Mn oxide barrier at 90 cm depth, gravel contributed a significant fraction of the total distribution (~42% gravel, ~34% sand and ~20% silt) and was more prevalent in the layers directly above and below the barrier (Fig. 3). In P2, the soil layers were generally more variable in composition with depth compared to those in P1, and in contrast to P1, the Mn oxide barrier at 60 cm depth was comprised predominantly of sand (~55% sand, ~23% silt, ~16% silt and 5% gravel) (Fig. 3).

3.2 Total metal content and distribution in the Mn oxide barriers

Total digestion of the soil from the different layers in the soil profiles revealed a pronounced enrichment in Mn coincident with the visual identification of black Mn oxide

barriers in P1 and P2 at 90 cm and 60 cm depth, respectively (Fig. 2). In both soil profiles, there was a relative enrichment in Fe either coincident with the Mn oxide barrier layer (P1, where enrichment began at 75 cm depth and continued until the groundwater table) or immediately after the barrier layer (P2, where enrichment began at 65 cm depth and continued until the groundwater table). Iron enrichments were coincident with an enhanced reddish-brown colour of the soil, and likely due to precipitation of iron (hydr)oxide minerals.

Data from the sequential extractions of the different soil layers revealed that the highest concentrations of Ba, Ni, Co, Cd, Zn and Ce (2643 ±105 µg g^{-1}, 257 ±9 µg g^{-1}, 127 ±4 µg g^{-1}, 12 ±0.5 µg g^{-1}, 147 ±6 µg g^{-1}, 93 ±4 µg g^{-1}, respectively, in P1, and 2075 ±62 µg g^{-1}, 223 ±9 µg g^{-1}, 61 ±2 µg g^{-1}, 3.8 ±0.2 µg g^{-1}, 113 ±4 µg g^{-1}, 84 ±3 µg g^{-1}, respectively, in P2) were present in the Mn oxide barrier layers (Fig. 3). Relatively high total Zn and Ce concentrations were also found in the soil layers above and below the Mn oxide barrier in P1, while in P2 total Ce concentrations varied little throughout the profile and were equivalent to those in the barrier at 75 cm depth. In detail the sequential extractions showed that in the Mn oxide barrier layers, Ba, Ni, Co and Cd were preferentially associated with the Mn oxide fraction (F3) (where for Ba 73% (P1) and 86% (P2) of total Ba was extracted in F3, and for Ni 69% (P1) and 82% (P2), for Co 84% (P1) and 85% (P2), and for Cd 82% (P1) and 72% (P2), were all extracted in F3). In the Mn oxide barrier layers, Zn and Ce were also found associated with the Mn oxide fraction, however, in all layers, the highest concentrations of these two metals were found in the residual fraction (F7).

Despite the likely occurrence of Fe oxyhydroxides in the soil layers, either coincident with the Mn oxide barrier layer (P1) or immediately after the barrier layer (P2), the sequential extractions for amorphous (F5) and crystalline (F6) Fe oxides showed that the measured elements were largely preferentially sequestered by Mn, rather than Fe, (hydr)oxides. Furthermore, in keeping with the low total carbon content of the soil profiles, organic compounds (F4) appeared to be the least important sorbents for the elements investigated (Fig. 3).

3.3 Geochemical modelling of soil solutions in Mn oxide barriers

Thermodynamic speciation calculations for Mn present in the soil solution in the Mn oxide barrier layers predicted Mn present as Mn^{2+}(aq) (75.5%) and $MnSO_4$(aq) (24.4%). All other Mn solution species contributed just 0.1%. Solid abiotic Mn species were significantly

undersaturated, with a saturation index of -10.4 for commonly occurring birnessite. As such, under the geochemical conditions present in the Mn oxide barrier soil solutions, the chemical oxidation of Mn, and thus the abiotic precipitation of birnessite, is thermodynamically unfavorable.

3.4 Manganese mineralogy in Mn oxide barriers

Backscattered electron images of the thin sections prepared from P1 and P2 Mn oxide barriers (Fig. 4), combined with electron microprobe spot analyses (Table 4), revealed Mn-bearing minerals (labelled A, Fig. 4) with minor amounts of Fe-bearing minerals (labelled B, Fig. 4) occurring as coatings on, and as infill between, Si-bearing mineral grains (labelled Q, Fig. 4). In comparison to the Fe-bearing and Si-bearing minerals, the Mn-bearing minerals (point A, Table 4) had measureable concentrations of Ca, Ba and Ni. SEM of the Mn-bearing minerals in the Mn oxide barriers revealed layer-like Mn mineral structures, matching those typically observed for birnessite-type minerals (e.g., Bargar et al., 2009a).

The SR-XRD spectrum of the bulk soil from the P2 Mn oxide barrier (Fig. 5) showed well defined peaks arising from quartz and muscovite and (or) kaolinite. In contrast to these, relatively weak peaks also arose matching the Mn oxide birnessite (for reference pattern see turbostratic birnessite, Drits et al., 1997) at ~7.10 [001], 3.50 [002], 2.42 [100] and 1.42 [110] Å (~12.4, 25.4, 37.1 and 65.7 $^{o}2\Theta$, respectively). The [001] and [002] reflections are weak and broad compared to synthetic crystalline birnessite (e.g., Peacock and Sherman, 2007) indicating that the birnessite is only semi-coherently stacked along the c-axis, and is thus poorly crystalline (e.g., Grangeon et al., 2010). In addition, d_{100}/d_{110} approximately equals $\sqrt{3}$, indicating that the birnessite has hexagonal symmetry.

To further determine the crystallinity and mineralogy of the birnessite, we performed Mn K-edge EXAFS spectroscopy, where the background-subtracted k^3-weighted EXAFS spectrum from the study site and the reference spectra (δ-MnO_2, hexagonal birnessite and triclinic birnessite) are shown in Figure 6. δ-MnO_2 is a hexagonal phyllomanganate with turbostratic c-axis stacking, and is therefore a very poorly crystalline version of birnessite. Mn EXAFS spectroscopy is sensitive to Mn-O and Mn-Mn interatomic distances, and MnO_6 polyhedral linkages (Manceau and Combes, 1988). Information on sample crystallinity and mineralogy can therefore be obtained by comparing sample spectra to a suite of standard Mn oxide reference

spectra (Manceau et al., 2002). In agreement with previous studies, our Mn oxide reference spectra show clear differences in k-space in the (6 – 10 $Å^{-1}$) indicator region (Webb et al., 2005a). This region is sensitive to the amount and ordering of Mn(IV) and Mn(III) in the sheets of phyllomanganates (δ-MnO_2, hexagonal birnessite and triclinic birnessite) (Manceau and Combes, 1988; McKeown and Post, 2001). In particular, the k-space features at ~ 6.1, 8.5, 9 and 9.6 $Å^{-1}$ appear sharper and more intense with an increase in coherent stacking of the layers along the c-axis, i.e., from δ-MnO_2 to hexagonal birnessite (Webb et al., 2005a). In addition, triclinic birnessite has a clear splitting of the features at ~ 8.5 and 9.6 $Å^{-1}$. In this regard, the Mn spectrum recorded for the P2 Mn oxide appears most similar to δ-MnO_2 and hexagonal birnessite. In agreement with the XRD and SEM, a slight decrease in the amplitude of the spectral features at ~ 8.5, 9 and 9.6 $Å^{-1}$ compared to hexagonal birnessite indicates that the Mn-bearing mineral in the Mn oxide barrier layers is a poorly crystalline hexagonal birnessite.

3.5 Identification of Mn(II)-oxidizing bacteria from Mn oxide barriers

Bacterial strains isolated from the surface layers of profiles P1 and P2 and the Mn oxide barrier layers were tested for Mn oxidation. Only isolates from the Mn oxide barriers led to the growth of Mn(II)-oxidizing bacteria (MOB). Specifically, we could identify firmicutes, actinobacteria and proteobacteria with the ability to oxidize Mn in pure culture (Fig. 7). Specifically, we identified three Gram-positive firmicutes affiliated to Bacillus safensis, Bacillus altitudinis and Brevibacillus reuszeri. These bacteria are spore-forming and were able to oxidize Mn after initiating spore formation. We also identified two Gram-positive actinobacteria belonging to the genera Arthrobacter and Frondihabitans. Lastly, within the Gram-negative proteobacteria, we identified an isolate belonging to the genus Sphingomonas (Fig. 7). The identified MOB and their sequence similarity to the GenBank database are shown in Table 5.

SR-XRD of the precipitates produced by the MOB in the laboratory (Fig. 8) showed that, under the conditions established here, these bacteria precipitated poorly crystalline hexagonal birnessite (for reference pattern see turbostratic birnessite, Drits et al., 1997), very similar in mineralogy and crystallinity to the Mn oxides identified in the Mn geochemical barriers located in P1 and P2 (section 3.4). Specifically, Bacillus sp. Mn oxide shows an extremely weak and broad peak at ~ 7 Å [001] (~ 12 $^{o}2\Theta$), and possibly another at ~ 3.5 Å [002] (~ 25 $^{o}2\Theta$) as part of the broad hump at ~ 20 $^{o}2\Theta$ (present in all the biogenic Mn oxide spectra and due to the presence

of bacterial biomass (Villalobos et al., 2006)). Subsequent weak and broad peaks are apparent at ~ 2.43 Å [100] and 1.41 Å [110] (~ 37 and 65 $^{o}2\Theta$, respectively). These peaks confirm the presence of birnessite, and their weak and broad nature indicates that the birnessite is incoherently stacked along the c-axis, and is thus poorly crystalline, similar to the δ-MnO_2-like product precipitated by P. putida GB-1 and synthetic δ-MnO_2. Brevibacillus sp. Mn oxide only shows peaks at ~ 2.43 Å [100] and 1.41 Å [110] (~ 37 and 65 $^{o}2\Theta$, respectively) and is therefore turbostratic and thus more poorly crystalline than that of Bacillus sp., P. putida GB-1 and synthetic δ-MnO_2. For both Bacillus sp. and Brevibacillus sp. d_{100}/d_{110} approximately equals $\sqrt{3}$, indicating that the birnessite has hexagonal symmetry. LA-ICP-MS analysis of selected isolates grown on agar plates confirmed that Mn oxide precipitation was only associated with the bacterial biomass, and that the concentration profile of Ni was positively correlated with Mn (Fig. S1 and S2 Supplementary Information, respectively).

To date, these bacterial communities have only been identified as MOB in circumneutral pH environments (Carmichael et al., 2013; Santelli et al., 2014; Tebo et al., 2005; Templeton et al., 2005). This is the first study to identify these bacteria as MOB in an acidic soil environment.

4. Discussion

4.1 Biogenic precipitation of poorly crystalline hexagonal birnessite at acidic soil pH

A significant number of recent studies indicate that poorly crystalline Mn oxides in natural environments are mostly of biogenic origin, formed via the microbial oxidation of Mn(II) (Bargar et al., 2009a; Chapnick et al., 1982; Granina and Mats, 2010; Miller et al., 2012; Nagy et al., 1991; Tebo et al., 2004). To date, MOB have been identified within several of the bacterial phyla, namely firmicutes, actinobacteria and proteobacteria (Akob et al., 2014; Carmichael et al., 2013; Santelli et al., 2013; Tebo et al., 2005; Xuezheng et al., 2008; Zakharova et al., 2010), and a number of studies have precipitated synthetic biogenic Mn oxides in the laboratory using different MOB, including, Leptothrix discophora SS-1 (Nelson et al., 1999), Pseudomonas putida GB-1 (Tebo et al., 2005; Zhu et al., 2010), Bacillus SG-1 (Bargar et al., 2005b; Webb et al., 2005a), Pseudomonas putida MnB1 (Villalobos et al., 2003) and Acremonium sp. KR21-2 (Tanaka et al., 2010). On the whole these MOB-produced laboratory Mn oxides have been identified as poorly crystalline hexagonal birnessite, most similar to synthetic δ-MnO_2. However,

in all the cases above where natural biogenic Mn oxides have been reported, and MOB have been used to produce laboratory biogenic Mn oxides, the pH has been measured or maintained at neutral to alkaline. To our knowledge, there is only one very recent report of biogenic Mn oxide precipitation at acidic pH in the environment, where two MOB have been isolated from our "Gessenhalde" study site at pH 5.5, Duganella isolate AB_14 and Albidiferax isolate TB-2, and cultured at pH 5.5 to produce Mn oxides with similarities to todorokite and birnessite (Akob et al., 2014). Other than this recent work, only three studies report the precipitation of MOB-produced laboratory Mn oxides at acidic pH (Bromfield, 1976; Bromfield, 1979; Ivarson and Heringa, 1972).

In order to elucidate the origin of the Mn oxides in the (bio)geochemical barriers at our site, we characterised the Mn oxide mineralogy present in the Mn oxide layers in two soil profiles, isolated and characterised MOB also present in the Mn oxide layers, and determined the physicochemical parameters throughout each profile. Characteristaion of the Mn oxide present in the Mn oxide barriers reveals the presence of poorly crystalline hexagonal birnessite (Fig. 5 and 6). This phase is very similar mineralogically and morphologically to δ-MnO_2, which is in turn the closest mineralogical match to biogenic Mn oxides reported in the literature (Bargar et al., 2005b; Villalobos et al., 2006; Villalobos et al., 2003; Webb et al., 2005a). Isolation and characterstaion of MOB present in the Mn oxide barriers reveals six strains of MOB (Table 5), which we subsequently culture to produce poorly crystalline hexagonal birnessite (Fig. 8), closely matching the Mn oxide identified in the Mn oxide barriers and typical biogenic Mn oxides. As discussed above, with the exception of Akob et al. (2014), biogenic poorly crystalline Mn oxides are typically identified in natural environments with circumneutral to alkaline pH (Bargar et al., 2009a; Chapnick et al., 1982; Granina and Mats, 2010; Miller et al., 2012; Nagy et al., 1991; Tebo et al., 2004). However, detailed soil profiling reveals an acidic soil pH in the Mn oxide barrier layers between pH 4.7 ±0.2 – 5.1 ±0.2 (pH 4.7 P1; pH 5.1 P2). Furthermore, geochemical thermodynamic modelling shows that the environmental conditions (pH, Eh) present in the Mn oxide barriers are thermodynamically unfavourable for the chemical oxidation of Mn(II). Taking all our results together, and in agreement with Akob et al. (2014), we suggest that the Mn oxides in the (bio)geochemical barriers at our study site are biogenically precipitated in an acidic soil environment. Precipitation of biogenic Mn oxides under acidic pH is an important result that extends our knowledge of microbial Mn(II) oxidation in natural and

contaminated soils and sediments. Furthermore, in addition to Akob et al. (2014), we identify six MOB strains at the "Gessenhalde" site that have previously only been identified as MOB in circumneutral pH environments (Carmichael et al., 2013; Santelli et al., 2014; Tebo et al., 2005; Templeton et al., 2005). This is the first study to identify these bacteria as MOB in an acidic soil environment, and thus also contributes to our knowledge of microbial Mn(II) oxidation in the environment. Lastly, of our identified strains, Bacillus sp. and Brevibacillus sp. in particular are spore-forming bacteria, and to our knowldege this is the first report to isolate spore-forming MOB from an acidic soil environment. In light of our work, it appears that dormant spores of Mn(II)-oxidizing bacteria are still able to catalyse Mn(II) oxidation. This necessitates further work on the microbial mechanisms of Mn(II) oxidation and mineralization by spores, and a revised assessment of the role and functions of dormant spores in the environment.

4.2 Biogenic Mn oxide barrier influence on trace metal abundance and distribution

In profile P1, wherever Mn is present in the soil (80 – 105 cm depth, as measured by total digest; Fig. 2), Ba, Ni, Co and Cd are preferentially associated with the Mn oxide fraction (F3) over the Fe oxide fractions (amorphous F4; crystalline F5) in all but two cases (Ni at 95 cm and 105 cm depth) (Fig. 3). In profile P2, where Mn is present (at low levels throughout the profile with a maximum at 60 cm depth, as measured by total digest; Fig. 2) Ba, Ni, Co and Cd are preferentially associated with the Mn oxide fraction (F3) in the Mn oxide barrier layer (60 cm depth), however either side of the barrier layer Ni is associated with crystalline Fe oxides (F6) over Mn oxides, and post barrier layer (65 – 90 cm depth) Co is somewhat more concentrated with Fe oxides (amorphous F5 and crystalline F6) than Mn oxides (Fig. 3). Importantly, in both profiles, these metals are overwhelmingly associated with the Mn oxide fraction in the barrier layers, despite the fact that, based on the total digest results and assuming all measured Mn and Fe in the barrier layers are present as poorly crystalline birnessite (δ-MnO_2) and ferrihydrite ($FeOOH.4H_2O$), there is a significantly smaller mass of birnessite compared to ferrihydrite available for metal sequestration (in P1 and P2 ~ 0.03 g δ-MnO_2 per g soil compared to P1 ~ 0.13 g and P2 ~ 0.05 g $FeOOH.4H_2O$ per g soil).

Further insight into the preferential distribution of metals between the Mn and Fe fractions can be gained by closer inspection of our total digest and sequential extraction results post barrier layer in P2 (from 65 – 90 cm depth), where we measure Mn at only very low levels

but significantly elevated Fe (Fig. 2). Again, assuming all measured Mn and Fe in this profile section are present as poorly crystalline birnessite (δ-MnO_2) and ferrihydrite ($FeOOH.4H_2O$), then our measured Mn and Fe concentrations equate to ~ 0.0006 g δ-MnO_2 per g soil (average present over 65 – 90 cm depth) and ~ 0.08 g (at 65 cm depth) to ~ 0.15 g (at 90 cm depth) $FeOOH.4H_2O$ per g soil. In this profile section, Ni is preferentially associated with crystalline Fe oxides (F6) over Mn oxides (Fig. 3), however, although Co is somewhat more concentrated with Fe oxides (amorphous F5 and crystalline F6) than Mn oxides, there is still significant Co association with Mn oxides, despite their very low abundance relative to Fe (hydr)oxides. As such there appears to be a dichotomy in the sorption behaviour of Ni and Co, where Co in particular is disproportionately associated with Mn oxides.

The abundance and distribution of these metals between the Mn and Fe (hydr)oxide fractions in part reflects the inherent differences in the surface sorption properties of these sorbent phases at the acidic soil pH of the barriers (pH 4.7 P1; pH 5.1 P2). Specifically, in the Mn oxide barriers, the dominant (inorganic) speciation of Ba, Ni, Co and Cd in the barrier porewater solutions is predicted to be Ba^{2+}(aq), Ni^{2+}(aq), Co^{2+}(aq) and Cd^{2+}(aq) while the point of zero charge for poorly crystalline birnessite is at ~ pH 2 (e.g., Catts and Langmuir, 1986) and for ferrihydrite at pH ~ 8 (e.g., Moon and Peacock, 2013). Thus, despite the lower abundance of Mn oxide relative to Fe (hydr)oxide in the barrier layers, providing the Mn oxide sorption capacity is not exceeded, then birnessite should effectively out compete ferrihydrite for metal cations at acidic pH (see for example the colloid-chemical model for the formation of ferromanganese precipitates in seawater, Koschinsky and Halbach, 1995). Indeed, from available studies to date at pH ~ 4.5 – 5 and in low ionic strength electrolytes designed to mimic freshwaters and soil porewaters (and where sorption capacities are not exceeded), there is near complete removal of Co and Ni from solution by birnessite (e.g., Peacock and Sherman, 2007; Murray, 1975) and only 30 – 50 % removal of Ni from solution by ferrihydrite (e.g., Trivedi and Axe, 2000).

Post barrier layer in P2, we observe what appears to be an interplay between the differences in the sorption properties of the sorbents, and the abundance of each sorbent phase relative to the other. In this profile section, where the abundance of the strongest sorbent is very limited, Ni is found exclusively associated with Fe (hydr)oxides, where work to date shows it is adsorbed as a Ni(II) surface adsorption complex (e.g., Xu et al., 2007). On the other hand, Co

(Manceau et al., 1997), Cr (Manceau and Charlet, 1991), Tl (Peacock and Moon, 2012) and Ce (Takahashi et al., 2007) are adsorbed and then oxidized by birnessite, resulting in strongly bound surface or structurally incorporated complexes. In marine ferromanganese precipitates, oxidative scavenging of Co likely explains the enhanced enrichment of Co over Ni (where in ferromanganese crusts Co and Ni are enriched ~ 255 and ~ 70 times over crustal values (e.g., Hein et al., 2013)). Thus similarly, despite only a limited abundance of Mn oxide in this profile section, the oxidative scavenging of Co vs. the simple adsorption of Ni likely explains the fact that Co is distributed between the Fe and Mn fractions while Ni is not. Oxidative scavenging of Ce by Mn oxide also likely explains the minor concentration of this element in the Mn fraction of the Mn oxide barrier layers in P1 and P2 (Fig. 3). This enrichment is similar to that observed in weathered rock from Koongarra, Australia, where Ce occurs as microcrystalline oxide globules on Mn mineral surfaces (Koppi et al., 1996), due to the oxidation of Ce(III) to Ce(IV) resulting in the formation of CeO_2 (Ohta and Kawabe, 2001).

In summary, biogenic precipitation of poorly crystalline hexagonal birnessite and the subsequent formation of (bio)geochemical barriers at acidic pH has lead to the extemely efficient immobilization of heavy metals at our mining-impacted study site. This kind of Mn oxide precipitation may be applied in biogeotechnologies for heavy metal remediation in contaminated soils and groundwaters, such as engineered in situ clean-up or (enhanced) natural attenuation via exploitation of (bio)geochemical barriers (e.g., Coldewey and Klinger, 2000; Ott, 2000; Peng et al., 2009).

Acknowledgements

This work was financially supported by the German Research Foundation (DFG) under the grant GRK 1257/2: “Alteration and element mobility at the microbe-mineral interface”. We thank Andrea Beyer, Dr. Daniel Mirgorodsky, Dr. Matthias Gube and Dr. Ralph Bolanz (Institute of Microbiology and Institute of Geosciences, Friedrich Schiller University, Jena, Germany) for their helpful contributions to the work presented here. We also thank Diamond Light Source Ltd. UK, for access to beamlines I11 and B18 (proposals EE3899 and SP9203) that contributed to the results presented here, and support at these beamlines from Andy Dent, Giannantonio Cibin, Steven Parry, Chiu Tang, Stephen Thompson and Claire Murray. Finally we thank the reviewers and associate editors for their helpful comments to improve the manuscript.

References

Akob, D.M., Bohu, T., Beyer, A., Schäffner, F., Händel, M., Johnson, C.A., Merten, D., Büchel, G., Totsche, K.U., Küsel, K., 2014. Identification of Mn(II)-oxidizing bacteria from a low pH contaminated former uranium mine. Applied and Environmental Microbiology. Doi: 10.1128/AEM.01296-14.

Anderson, C., Davis, R., Bandolin, N., Baptista, A., Tebo, B., 2011. Analysis of in situ manganese (II) oxidation in the Columbia River and offshore plume: linking Aurantimonas and the associated microbial community to an active biogeochemical cycle. Environmental Microbiology, 13(6): 1561-1576.

Anderson, C. et al., 2009. Mn (II) oxidation is catalyzed by heme peroxidases in "Aurantimonas manganoxydans" strain SI85-9A1 and Erythrobacter sp. strain SD-21. Applied and Environmental Microbiology, 75(12): 4130-4138.

Bargar, J.R et al., 2009a. Structural characterization of terrestrial microbial Mn oxides from Pinal Creek, AZ. Geochimica et Cosmochimica Acta, 73(4): 889-910.

Bargar, J.R, Webb, S., Tebo, B., 2005a. EXAFS, XANES and in-situ SR-XRD characterization of biogenic manganese oxides produced in sea water. Physica Scripta, 2005: 888.

Bargar, J.R. et al., 2009b. Structural characterization of terrestrial microbial Mn oxides from Pinal Creek, AZ. Geochimica et Cosmochimica Acta, 73(4): 889-910.

Bargar, J.R. et al., 2005b. Biotic and abiotic products of Mn (II) oxidation by spores of the marine Bacillus sp. strain SG-1. American Mineralogist, 90(1): 143-154.

Bargar, J.R., Tebo, B.M., Villinski, J.E., 2000. In situ characterization of Mn (II) oxidation by spores of the marine Bacillus sp. strain SG-1. Geochimica et Cosmochimica Acta, 64(16): 2775-2778.

Bradl, H.B., 2004. Adsorption of heavy metal ions on soils and soils constituents. Journal of Colloid and Interface Science, 277(1): 1-18.

Bromfield, S.M, 1976. The deposition of manganese oxide by an alga on acid soil. Soil Research, 14(1): 95-102.

Bromfield, S.M., 1978. The effect of manganese-oxidizing bacteria and pH on the availability of manganous ions and manganese oxides to oats in nutrient solutions. Plant and Soil, 49(1): 23-39.

Bromfield, S.M., 1979. Manganous ion oxidation at pH values below 5.0 by cell-free substances from Streptomyces sp. Cultures. Soil Biology and Biochemistry, 11(2): 115-118.

Brouwers, G., Vijgenboom, E., Corstjens, P., De Vrind, J., De Vrind-De Jong, E., 2000. Bacterial Mn^{2+} oxidizing systems and multicopper oxidases: an overview of mechanisms and functions. Geomicrobiology Journal, 17(1): 1-24.

Burkhardt, E.M., Meißner, S., Merten, D., Büchel, G., Küsel, K., 2009. Heavy metal retention and microbial activities in geochemical barriers formed in glacial sediments subjacent to a former uranium mining leaching heap. Chemie der Erde-Geochemistry, 69: 21-34.

Burns, V.M., Burns, R.G., 1978. Post-depositional metal enrichment processes inside manganese nodules from the north equatorial Pacific. Earth and Planetary Science Letters, 39(3): 341-348.

Büchel, G., Merten, D., 2009. Geo-Bio-Interactions at heavy-metal-contaminated sites. Chemie der Erde - Geochemistry, 69, Supplement 2(0): 1-3.

Carlsson, E., Büchel, G., 2005. Screening of residual contamination at a former uranium heap leaching site, Thuringia, Germany. Chemie der Erde - Geochemistry, 65, Supplement 1(0): 75-95.

Carmichael, M.J., Carmichael, S.K., Santelli, C.M., Strom, A., Bräuer, S.L., 2013. Mn (II)-oxidizing bacteria are abundant and environmentally relevant members of ferromanganese deposits in caves of the upper Tennessee River Basin. Geomicrobiology Journal, 30(9): 779-800 .

Chapnick, S.D., Moore, W.S., Nealson, K.H., 1982. Microbially mediated manganese oxidation in a freshwater lake. Limnology and Oceanography, 27(6): 1004-1014.

Coldewey, W.G. and Klinger, C., 2000. Characterization of the Geological and Hydrogeological Situation, Effects on Natural Geochemical Barriers and Remediation. Biotechnology: Environmental Processes II, Second Edition: 11b:43-59.

Crerar, D.A., Barnes, H.L., 1974. Deposition of deep-sea manganese nodules. Geochimica et Cosmochimica Acta, 38(2): 279-300.

Drits, V.A., Silvester, E., Gorshkov, A.L. and Manceau, A., 1997. Structure of synthetic monoclinic Na-rich birnessite and hexagonal birnessite: I. Results from X-Ray diffraction and selected area electron diffraction. American Mineralogist 82: 946-961.

Feng, X.H. et al., 2010. Formation of nano-crystalline todorokite from biogenic Mn oxides. Geochimica et Cosmochimica Acta, 74(11): 3232-3245.

Francis, C.A., Tebo, B.M., 2001. cumA multicopper oxidase genes from diverse Mn (II)-oxidizing and non-Mn (II)-oxidizing Pseudomonas strains. Applied and Environmental Microbiology, 67(9): 4272-4278.

Francis, C.A., Tebo, B.M., 2002. Enzymatic manganese (II) oxidation by metabolically dormant spores of diverse Bacillus species. Applied and Environmental Microbiology, 68(2): 874-880.

Fuller, C.C., Harvey, J.W., 2000. Reactive uptake of trace metals in the hyporheic zone of a mining-contaminated stream, Pinal Creek, Arizona. Environmental Science & Technology, 34(7): 1150-1155.

Grangeon, S., Lanson, B., Miyata, N., Tani, Y., Manceau, A., 2010. Structure of nanocrystalline phyllomanganates produced by freshwater fungi. American mineralogist, 95(11-12): 1608-1616.

Granina, L., Mats, V., 2010. Iron-Manganese nodules in lake baikal. Minerals of the Ocean-5 and Deep-sea minerals and Mining-2: 23-26.

Grawunder, A., Lonschinski, M., Merten, D., Büchel, G., 2009. Distribution and bonding of residual contamination in glacial sediments at the former uranium mining leaching heap of Gessen/Thuringia, Germany. Chemie der Erde-Geochemistry, 69: 5-19.

Hein, J.R., Mizell, K., Koschinsky, A., Conrad, T.A., 2013. Deep-ocean mineral deposits as a source of critical metals for high- and green-technology applications: Comparison with land-based resources. Ore Geology Reviews, 51: 1-14.

Hem, J.D., 1978. Redox processes at surfaces of manganese oxide and their effects on aqueous metal ions. Chemical Geology, 21(3–4): 199-218.

Hosseinkhani, B., Emtiazi, G., 2011. Synthesis and characterization of a novel extracellular biogenic manganese oxide (Bixbyite-like Mn_2O_3) nanoparticle by isolated Acinetobacter sp. Current microbiology, 63(3): 300-305.

Ivarson, K., Heringa, P., 1972. Oxidation of manganese by microorganisms in manganese deposits of Newfoundland soil. Canadian Journal of Soil Science, 52(3): 401-416.

Jakubick, A.T., Gatzweiler, R., Mager, D., MacG Robertson, A., 1997. The Wismut waste rock pile remediation program of the Ronneburg mining district, Germany, Proceedings of the

Fourth International Conference on Acid Rock Drainage, Vancouver, B.C. Canada: 1285 -1301.

Koppi, A.J. et al., 1996. Rare earth element trends and cerium-uranium-manganese associations in weathered rock from Koongarra, Northern Territory, Australia. Geochimica et Cosmochimica Acta, 60(10): 1695-1707.

Lee, G., Bigham, J.M., Faure, G., 2002. Removal of trace metals by coprecipitation with Fe, Al and Mn from natural waters contaminated with acid mine drainage in the Ducktown Mining District, Tennessee. Applied Geochemistry, 17(5): 569-581.

Lehmann, R., Cheng, H., Harsh, J., 1987. Oxidation of phenolic acids by soil iron and manganese oxides. Soil Science Society of America Journal, 51(2): 352-356.

Luan, F., Santelli, C.M., Hansel, C.M., Burgos, W.D. 2012. Defining manganese(II) removal processes in passive coal mine drainage treatment systems through laboratory incubation experiments. Applied Geochemistry 27: 1567-1578.

Manceau, A., Charlet, L., 1992. X-ray absorption spectroscopic study of the sorption of Cr (III) at the oxide-water interface: I. Molecular mechanism of Cr (III) oxidation on Mn oxides. Journal of Colloid and Interface Science, 148(2): 425-442.

Manceau, A., Combes, J., 1988. Structure of Mn and Fe oxides and oxyhydroxides: a topological approach by EXAFS. Physics and Chemistry of Minerals, 15(3): 283-295.

Manceau, A and Charlet, L., 1992. X-ray absorption spectroscopic study of the sorption of Cr(III) at the oxide-water interface: 1. Molecular mechanism of Cr(III) oxidation on Mn oxides. Journal of Colloid and Interface Science, 148(2): 425-442.

Manceau, A., Drits, V.A., Silvester, E., Bartoli, C., Lanson, B., 1997. Structural mechanism of Co^{2+} oxidation by the phyllomangante buserite. American Mineralogist, 82: 1150-1175.

Manceau, A., Kersten, M., Marcus, M.A., Geoffroy, N., Granina, L., 2007. Ba and Ni speciation in a nodule of binary Mn oxide phase composition from Lake Baikal. Geochimica et Cosmochimica Acta, 71(8): 1967-1981.

Manceau, A., Llorca, S., Calas, G., 1986. Structural chemistry of Mn, Co and Ni in some natural manganese oxides. Le Journal de Physique Colloques, 47: C8-703-C8-707.

Manceau, A., Marcus, M.A., Tamura, N., 2002. Quantitative speciation of heavy metals in soils and sediments by synchrotron X-ray techniques. Reviews in Mineralogy and Geochemistry, 49(1): 341-428.

Manceau, A. et al., 2003. Molecular-scale speciation of Zn and Ni in soil ferromanganese nodules from loess soils of the Mississippi Basin. Environmental Science & Technology, 37(1): 75-80.

Mandernack, K.W., Post, J., Tebo, B.M., 1995. Manganese mineral formation by bacterial spores of the marine Bacillus, strain SG-1: Evidence for the direct oxidation of Mn (II) to Mn (IV). Geochimica et Cosmochimica Acta, 59(21): 4393-4408.

McKenzie, R., 1981. The surface charge on manganese dioxides. Soil Research, 19(1): 41-50.

McKeown, D.A., Post, J.E., 2001. Characterization of manganese oxide mineralogy in rock varnish and dendrites using X-ray absorption spectroscopy. American Mineralogist, 86(5-6): 701-713.

Miller, A.Z. et al., 2012. Biogenic Mn oxide minerals coating in a subsurface granite environment. Chemical Geology, 322–323(0): 181-191.

Miyata, N., Tani, Y., Sakata, M., Iwahori, K., 2007. Microbial manganese oxide formation and interaction with toxic metal ions. Journal of Bioscience and Bioengineering, 104(1): 1-8.

Moon, E.M., Peacock, C.L., 2013. Modelling Cu(II) adsorption to ferrihydrite and ferrihydrite-bacteria composites: Deviation from additive adsorption in the composite sorption system. Geochimica et Cosmochimica Acta, 104: 148-164.

Morgan, J.J., 2005. Kinetics of reaction between O_2 and Mn (II) species in aqueous solutions. Geochimica et Cosmochimica Acta, 69(1): 35-48.

Murray, J.W., 1975. The interaction of metal ions at the manganese dioxide-solution interface. Geochimica et Cosmochimica Acta, 39(4):505-519.

Nagy, B. et al., 1991. Rock varnish in the Sonoran Desert: microbiologically mediated accumulation of manganiferous sediments. Sedimentology, 38(6): 1153-1171.

Nelson, Y.M., Lion, L.W., Ghiorse, W.C., Shuler, M.L., 1999. Production of biogenic Mn oxides by Leptothrix discophora SS-1 in a chemically defined growth medium and evaluation of their Pb adsorption characteristics. Applied and Environmental Microbiology, 65(1): 175-180.

Nelson, Y.M., Lion, L.W., Shuler, M.L., Ghiorse, W.C., 2002. Effect of oxide formation mechanisms on lead adsorption by biogenic manganese (hydr) oxides, iron (hydr) oxides, and their mixtures. Environmental Science & Technology, 36(3): 421-425.

Ohta, A., Kawabe, I., 2001. REE(III) adsorption onto Mn dioxide (δ-MnO_2) and Fe oxyhydroxide: Ce(III) oxidation by δ-MnO_2. Geochimica et Cosmochimica Acta, 65(5): 695-703.

Ott, N., 2000. Permeable reactive barriers for inorganics. USEPA, Washington DC.

Parkhurst, D.L., Appelo, C., 2013. Description of input and examples for PHREEQC version 3 • A computer program for speciation, batch-reaction, one-dimensional transport, and inverse geochemical calculations. US Geological Survey Techniques and Methods, Book 6, Modeling Techniques.

Peacock, C.L., 2009. Physiochemical controls on the crystal-chemistry of Ni in birnessite: Genetic implications for ferromanganese precipitates. Geochimica et Cosmochimica Acta, 73(12): 3568-3578.

Peacock, C.L., Moon, E.M., 2012. Oxidative scavenging of thallium by birnessite: Explanation for thallium enrichment and stable isotope fractionation in marine ferromanganese precipitates. Geochimica et Cosmochimica Acta, 84: 297-313.

Peacock, C.L., Sherman, D.M., 2007. Sorption of Ni by birnessite: Equilibrium controls on Ni in seawater. Chemical Geology, 238: 94-106.

Peacock, C.L., Sherman, D.M., 2004. Copper (II) sorption onto goethite, hematite and lepidocrocite: a surface complexation model based on ab initio molecular geometries and EXAFS spectroscopy. Geochimica et Cosmochimica Acta, 68(12): 2623-2637.

Peng, J.-f., Song, Y.-h., Yuan, P., Cui, X.-y., Qiu, G.-l., 2009. The remediation of heavy metals contaminated sediment. Journal of Hazardous Materials, 161(2–3): 633-640.

Perel'man, A., 1961. Geochemical principles of landscape classification. Soviet Geography, 2(3): 63-73.

Perel'man, A.I., 1967. Geochemistry of epigenesis. Plenum Press, New York: 266.

Perel'man, A.I., 1986. Geochemical barriers: theory and practical applications. Applied Geochemistry, 1(6): 669-680.

Post, J.E., 1999. Manganese oxide minerals: Crystal structures and economic and environmental significance. Proceedings of the National Academy of Sciences, 96(7): 3447.

Ravel, B., Newville, M., 2005. ATHENA, ARTEMIS, HEPHAESTUS: data analysis for X-ray absorption spectroscopy using IFEFFIT. Journal of Synchrotron Radiation, 12: 537-541.

Santelli, C.M., Chaput, D.L., Hansel, C.M., 2014. Microbial communities promoting Mn (II) oxidation in Ashumet Pond, a historically polluted freshwater pond undergoing remediation. Geomicrobiology Journal, 31(7): 605-616.

Santelli, C.M., Pfister, D.H., Lazarus, D., Sun, Lu., Burgos, W.D., Hansel, C.M. 2010. Promotion of Mn (II) oxidation and remediation of coal mine drainage in passive treatment systems by diverse fungal and bacterial communities. Applied and Environmental Microbiology, 76(14): 4871-4875.

Santelli, C.M., Webb, S.M., Dohnalkova, A.C., Hansel, C.M. 2011. Diversity of Mn oxides produced by Mn(II)-oxidizing fungi. Geochimica et Cosmochimica Acta, 75: 2762-2776.

Saratovsky, I., Wightman, P.G., Pastén, P.A., Gaillard, J.F., Poeppelmeier, K.R., 2006. Manganese oxides: Parallels between abiotic and biotic structures. Journal of the American Chemical Society, 128(34): 11188-11198.

Sherman, D.M., and Peacock, C.L., 2010. Surface complexation of Cu on birnessite (δ-MnO_2): Controls on Cu in the deep ocean. Geochimica et Cosmochimica Acta, 74(23): 6721-6730.

Spiro, T.G., Bargar, J.R., Sposito, G., Tebo, B.M., 2009. Bacteriogenic manganese oxides. Accounts of chemical research, 43(1): 2-9.

Takahashi, Y., Manceau, A., Geoffroy, N., Marcus, M.A., Usui, A., 2007. Chemical and structural control of the partitioning of Co, Ce, and Pb in marine ferromanganese oxides. Geochimica et Cosmochimica Acta, 71(4): 984-1008.

Tanaka, K. et al., 2010. A specific Ce oxidation process during sorption of rare earth elements on biogenic Mn oxide produced by Acremonium sp. strain KR21-2. Geochimica et Cosmochimica Acta, 74(19): 5463-5477.

Tebo, B.M. et al., 2004. Biogenic manganese oxides: properties and mechanisms of formation. Annu. Rev. Earth Planet. Sci., 32: 287-328.

Tebo, B.M., Johnson, H.A., McCarthy, J.K., Templeton, A.S., 2005. Geomicrobiology of manganese (II) oxidation. Trends in Microbiology, 13(9): 421-428.

Tebo, B.M., Clement, B.G., Dick, G.J., 2007. Biotransformations of manganese. Manual of environmental microbiology, 3rd ed. ASM Press, Washington, DC: 1223-1238.

Templeton, A.S., Staudigel, H., Tebo, B.M., 2005. Diverse Mn (II)-oxidizing bacteria isolated from submarine basalts at Loihi Seamount. Geomicrobiology Journal, 22(3-4): 127-139.

Tipping, E., Heaton, M., 1983. The adsorption of aquatic humic substances by two oxides of manganese. Geochimica et Cosmochimica Acta, 47(8): 1393-1397.

Trivedi, P., Axe, L., 2000. Modeling Cd and Zn sorption to hydrous metal oxides. Environmental Science & Technology, 34(11): 2215-2223.

Villalobos, M., Lanson, B., Manceau, A., Toner, B., Sposito, G., 2006. Structural model for the biogenic Mn oxide produced by Pseudomonas putida. American Mineralogist, 91(4): 489-502.

Villalobos, M., Toner, B., Bargar, J., Sposito, G., 2003. Characterization of the manganese oxide produced by Pseudomonas putida strain MnB1. Geochimica et Cosmochimica Acta, 67(14): 2649-2662.

Webb, S., Tebo, B., Bargar, J., 2005a. Structural characterization of biogenic Mn oxides produced in seawater by the marine Bacillus sp. strain SG-1. American Mineralogist, 90(8-9): 1342-1357.

Webb, S.M., Dick, G.J., Bargar, J.R., Tebo, B.M., 2005b. Evidence for the presence of Mn (III) intermediates in the bacterial oxidation of Mn (II). Proceedings of the National Academy of Sciences of the United States of America, 102(15): 5558-5563.

Xuezheng, L., Aiguo, G., Haowen, C., 2008. Isolation and phylogenetic analysis of cultivable manganese bacteria in sediments from the Arctic Ocean. Acta Ecologica Sinica, 28(12): 6364-6370.

Zakharova, Y.R., Parfenova, V., Granina, L., Kravchenko, O., Zemskaya, T., 2010. Distribution of iron-and manganese-oxidizing bacteria in the bottom sediments of Lake Baikal. Inland Water Biology, 3(4): 313-321.

Zeien, H., Brümmer, G.W., 1989. Chemische Extraktionen zur Bestimmung von Schwermetallbindungsformen in Böden. Mitteilungen Dt. Bodenkundl. Gesellsch, 59: 505-510.

Zhu, M., Ginder-Vogel, M., Parikh, S.J., Feng, X.H., Sparks, D.L., 2010. Cation effects on the layer structure of biogenic Mn-oxides. Environmental Science & Technology, 44(12): 4465-4471.

Xu, Y., Axe, L., Boonfueng, T., Tyson, T.A., Trivedi, P., Pandya, K., 2007. Ni(II) complexation to amorphous hydrous ferric oxide: An X-ray absorption spectroscopy study. J. Colloid Interf. Sci. 314: 10-17.

FIGURE & TABLE CAPTIONS

Figure 1: Map showing the Ronneburg district and the study sample site, where P1 and P2 indicate the locations of the study soil profiles, also showing the former leaching heaps, waste dumps and open pit mine.

Figure 2: Photograph of the soil profiles P1 and P2 identifying Mn oxide barrier layers at 90 cm and 60 cm depth, respectively. Line graphs show the pattern of physicochemical parameters (redox potential, electrical conductivity and pH) and corresponding metal concentrations measured by total digest for selected elements in different horizons in P1 and P2.

Figure 3: Graphical representation of grain size distribution and results of the sequential extractions for selected elements from the soil profiles P1 and P2.

Figure 4: Back scattered electron images (1, 2, 3 and 4) of Mn mineralization from the Mn oxide barriers in soil profiles P1 and P2, where areas labelled (A) are patchy and thread-like Mn oxides, (B) iron oxides and (Q) silicon dioxides. Electron microbe analyses at points A, B and Q are shown in Table 4. SEM images of the Mn-bearing minerals in the Mn oxide barriers (5 and 6) show sheet structure of Mn oxides.

Figure 5: SR-XRD for bulk soil samples from the Mn oxide barriers in soil profiles P1 and P2.

Figure. 6: Mn K-edge EXAFS spectra of the bulk soil from the Mn oxide barrier in soil profile P2. Reference spectra correspond to TB: Triclinic birnessite, HB: Hexagonal birnessite and D: δ-MnO_2.

Figure 7: Maximum-likelihood (ML) tree showing the phylogenetic relationships of Mn(II)-oxidizing bacteria isolated using 16S rRNA gene. Isolates from this study are shown in bold and the related strains from GenBank are shown in italics. ML tree was constructed with Treefinder Oct2010 using the generalized time reversible (GTR) nucleotide substitution model with 1,000 LR-ELW branch support replicates. Scale bar: 0.03 substitutions per nucleotide site.

Figure 8: SR-XRD spectra of biogenic Mn oxides: (A) produced by Bacillus sp., (B) produced by Brevibacillus sp., and reference Mn oxides synthesized for this work: (C) the δ-MnO_2-like product precipitated by P. putida GB-1, (D) synthetic δ-MnO_2, a poorly crystalline hexagonal birnessite. The broad hump at ~ 20 $^{o}2\theta$ in spectra A, B and C is due to the presence of bacterial biomass.

Table 1: Steps of the sequential extraction procedure of Zeien and Brümmer (1989).

Table 2: Input data for geochemical thermodynamic speciation modeling.

Table 3: Electrical conductivity, pH and total carbon content in the different layers of soil profiles P1 and P2.

Table 4: Chemical composition of polished thin sections prepared from the Mn oxide barrier layers in soil profiles P1 and P2, in weight percentage of major and minor elements from spot analyses (limit of detection = 0.1 wt %). The associated images and exact location of the analysed spots are shown in Fig. 4.

Table 5: Sequence similarity of isolated Mn(II)-oxidizing bacteria identified from the Mn oxide barrier layers in soil profiles P1 and P2.

Figure 1: Map showing the Ronneburg district and the study sample site, where P1 and P2 indicate the locations of the study soil profiles, also showing the former leaching heaps, waste dumps and open pit mine.

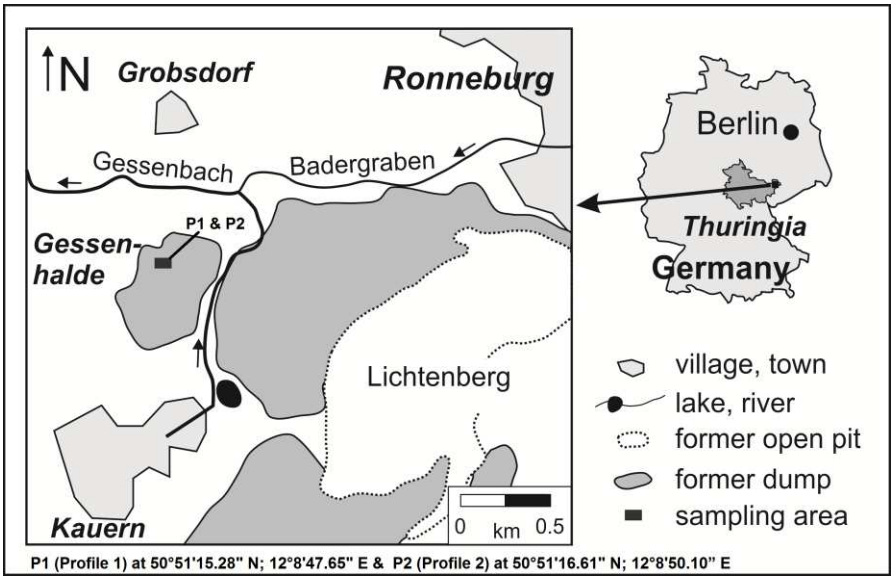

Figure 2: Photograph of the soil profiles P1 and P2 identifying Mn oxide barrier layers at 90 cm and 60 cm depth, respectively. Line graphs show the pattern of physicochemical parameters (redox potential, electrical conductivity and pH) and corresponding metal concentrations measured by total digest for selected elements in different horizons in P1 and P2.

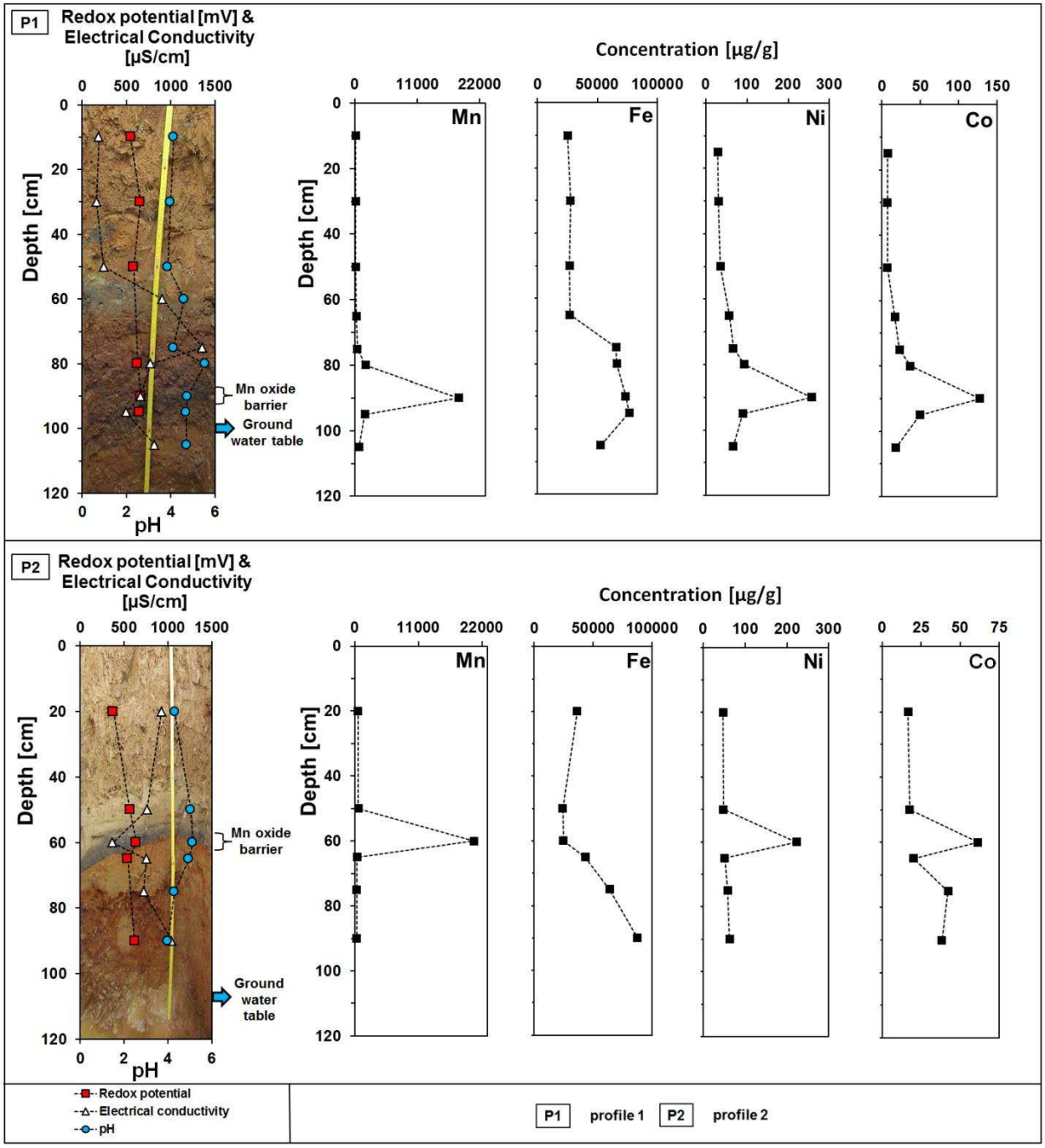

Figure 3: Graphical representation of grain size distribution and results of the sequential extractions for selected elements from the soil profiles P1 and P2.

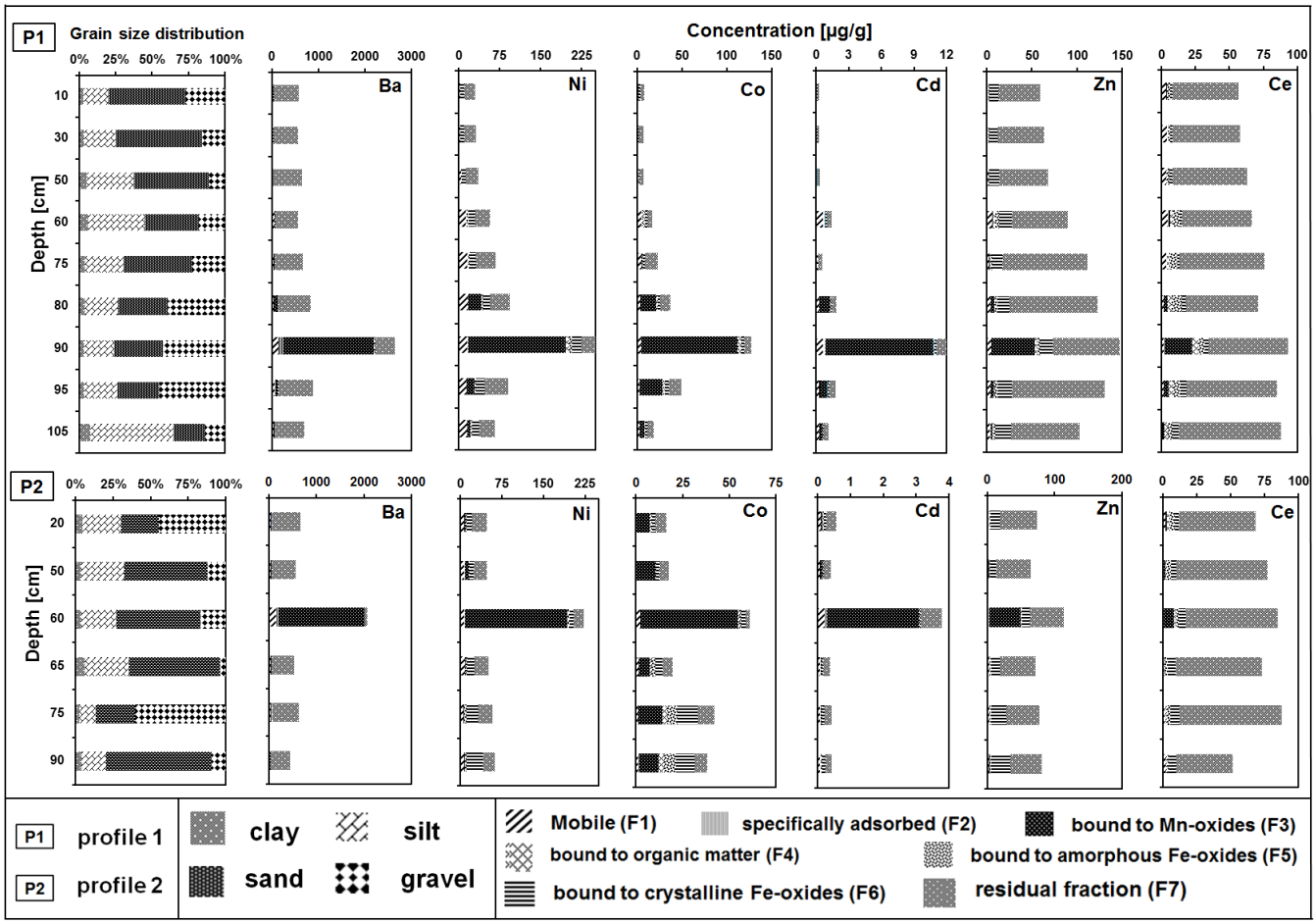

Figure 4: Back scattered electron images (1, 2, 3 and 4) of Mn mineralization from the Mn oxide barriers in soil profiles P1 and P2, where areas labelled (A) are patchy and thread-like Mn oxides, (B) iron oxides and (Q) silicon dioxides. Electron microbe analyses at points A, B and Q are shown in Table 4. SEM images of the Mn-bearing minerals in the Mn oxide barriers (5 and 6) show sheet structure of Mn oxides.

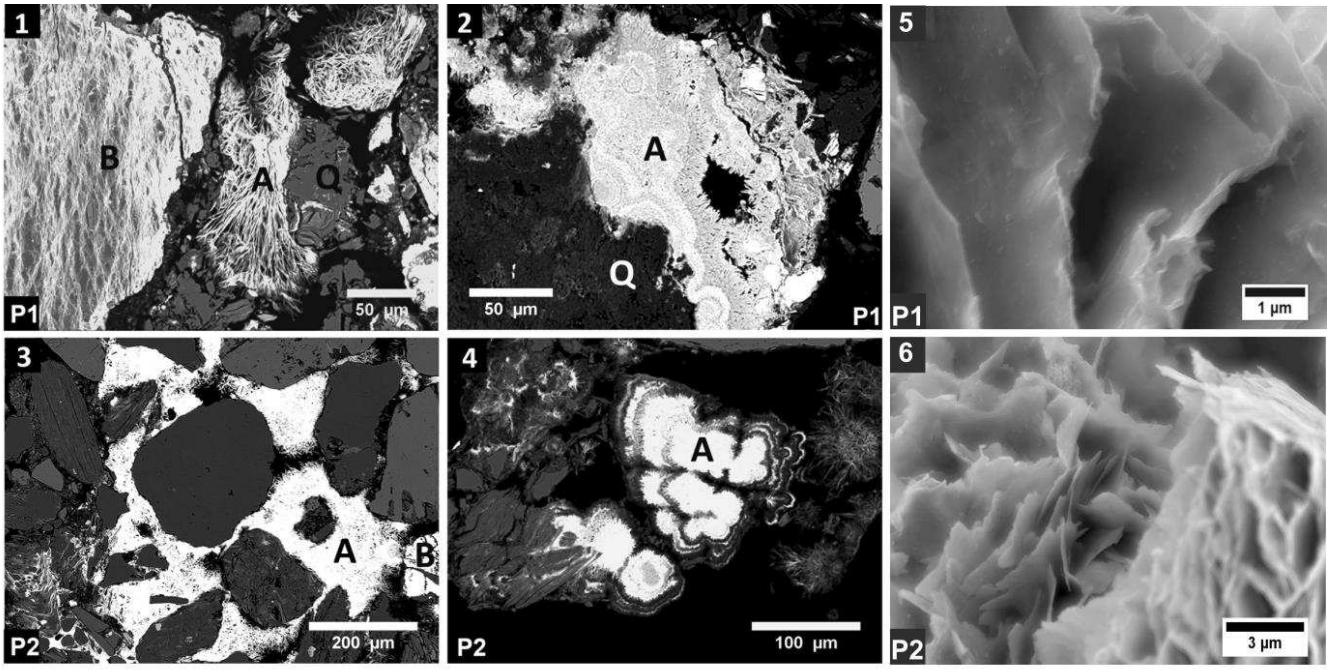

Figure 5: SR-XRD for bulk soil samples from the Mn oxide barriers in soil profiles P1 and P2.

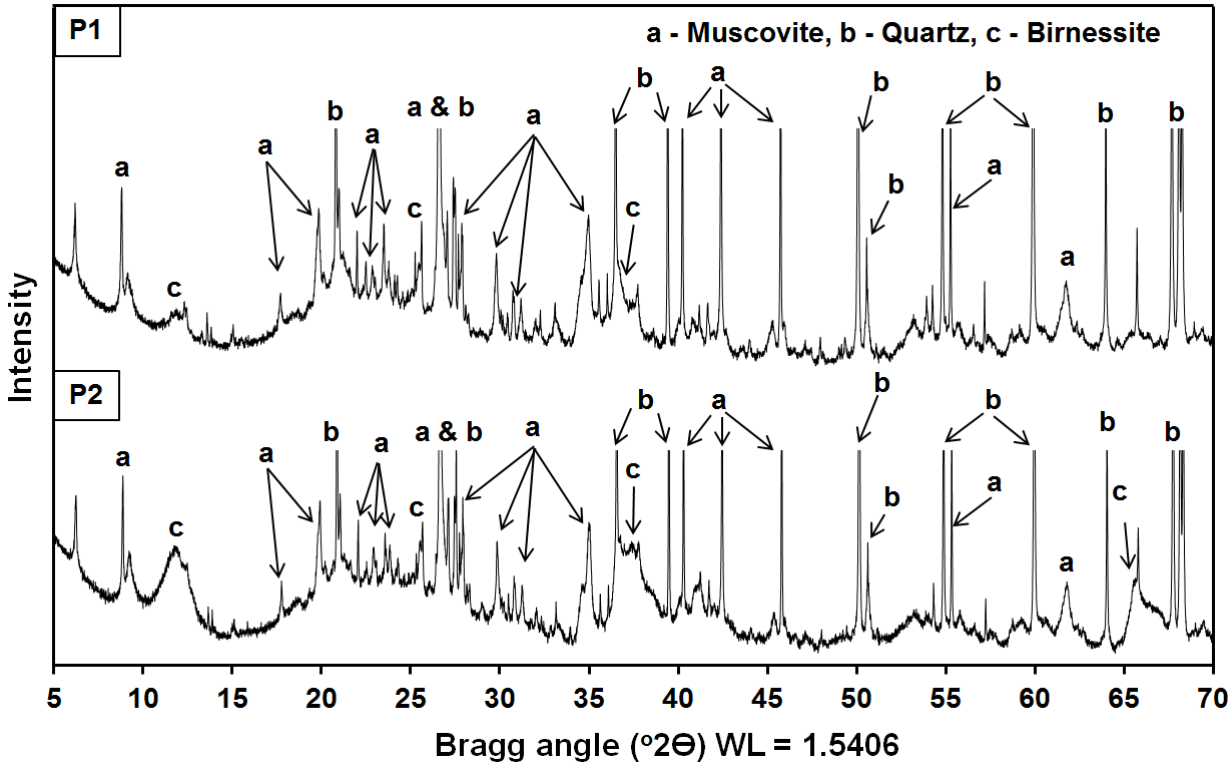

Figure. 6: Mn K-edge EXAFS spectra of the bulk soil from the Mn oxide barrier in soil profile P2. Reference spectra correspond to TB: Triclinic birnessite, HB: Hexagonal birnessite and D: δ-MnO_2.

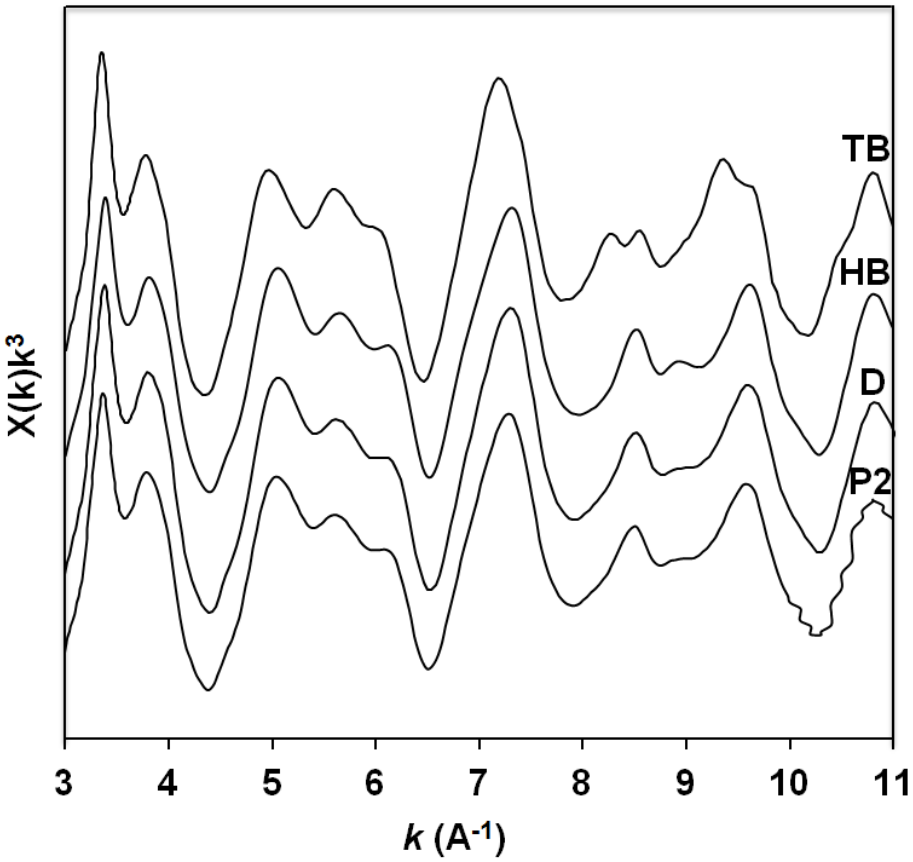

Figure 7: Maximum-likelihood (ML) tree showing the phylogenetic relationships of Mn(II)-oxidizing bacteria isolated using 16S rRNA gene. Isolates from this study are shown in bold non-italic text and the related strains from GenBank are shown in italics. ML tree was constructed with Treefinder Oct2010 using the generalized time reversible (GTR) nucleotide substitution model with 1,000 LR-ELW branch support replicates. Scale bar: 0.03 substitutions per nucleotide site.

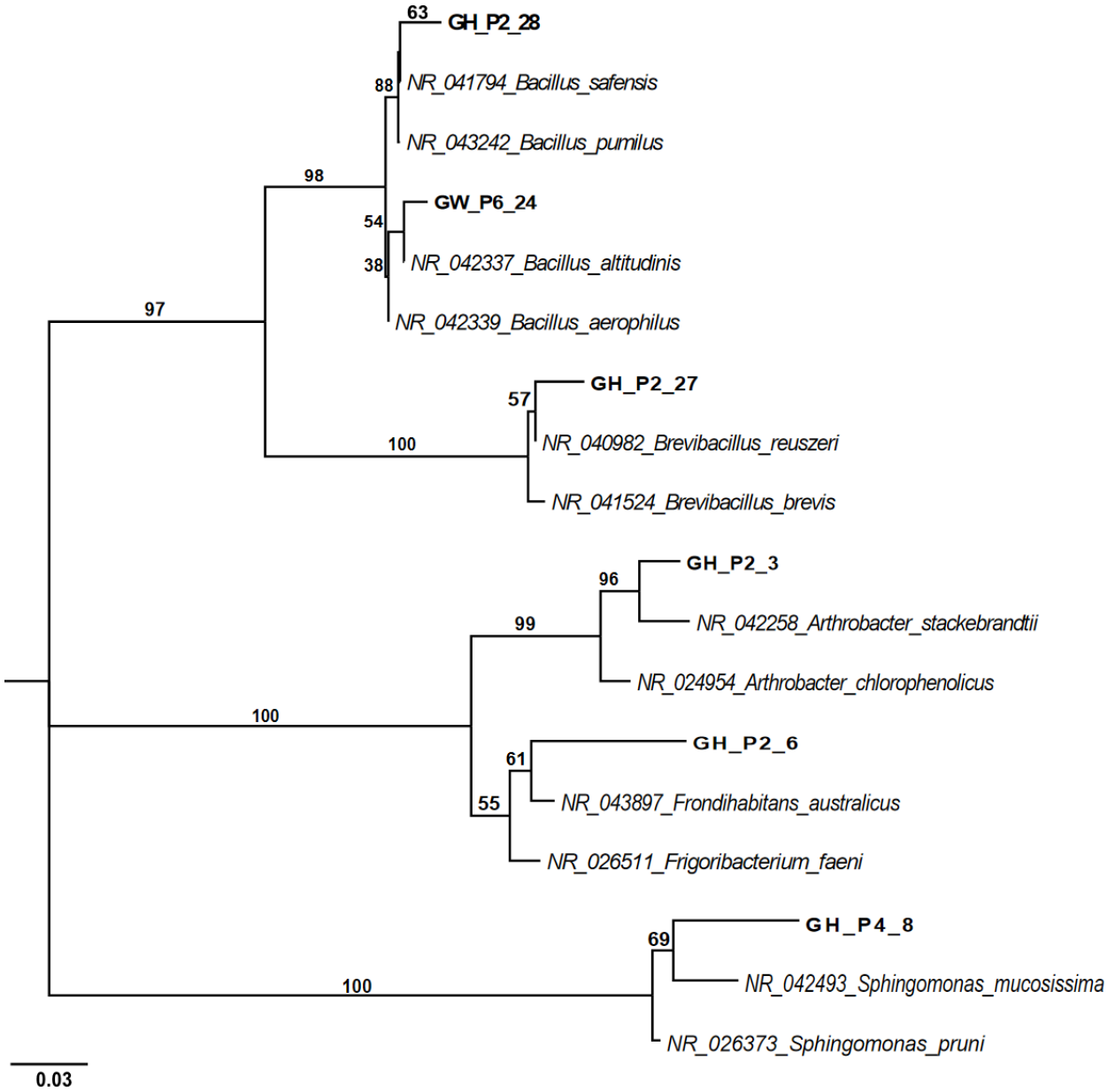

Figure 8: SR-XRD spectra of biogenic Mn oxides: (A) produced by Bacillus sp., (B) produced by Brevibacillus sp., and reference Mn oxides synthesized for this work: (C) the δ-MnO_2-like product precipitated by P. putida GB-1, (D) synthetic δ-MnO_2, a poorly crystalline hexagonal birnessite. The broad hump at ~ 20 $^{o}2\theta$ in spectra A, B and C is due to the presence of bacterial biomass.

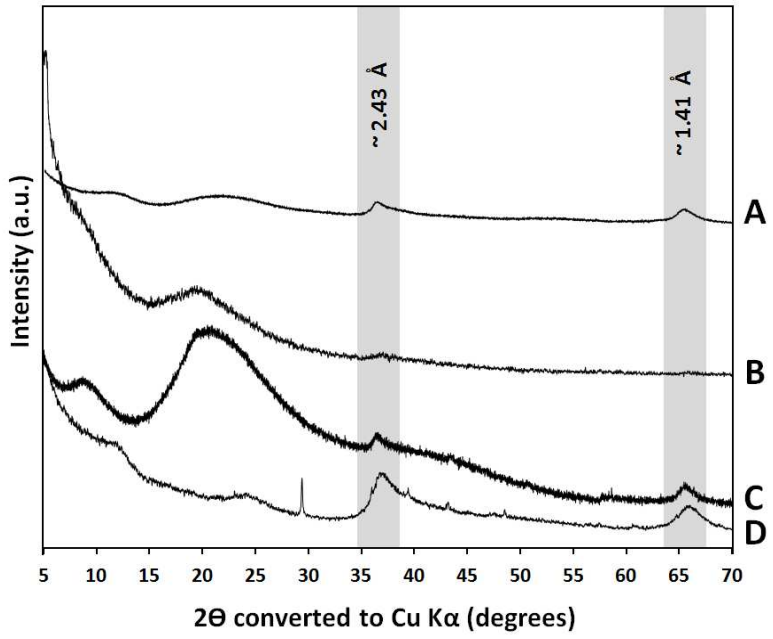

Table 1: Steps of the sequential extraction procedure of Zeien and Brümmer (1989).

Step	Extractant	Equilibration time	pH	Approximate nature of metal
F1	1M NH_4NO_3	24 h	natural	mobile
F2	1M NH_4-acetate	24 h	6.0	specifically adsorbed
F3	0.1M $NH_2OH.HCL$ + 1 M NH_4-acetate	30 min	6.0	bound to Mn oxides
F4	0.025M NH_4-EDTA	90 min	4.6	bound to organic matter
F5	0.2M NH_4-oxalate	04 h	3.25	bound to amorphous Fe oxides
F6	0.1M ascorbic acid in 0.2 M NH_4-oxalate	30 min in boiling water	3.25	bound to crystalline Fe oxides
F7	calculated from the results of total digestions and the sum of fractions F1-F6 from sequential extraction			residual fraction

Table 2: Input data for geochemical thermodynamic speciation modeling.

Parameters	**Profile 1**	**Profile 2**
	Concentration (μg L^{-1})	**Concentration (μg L^{-1})**
Electrical conductivity	658 (μS cm^{-1})	370 (μS cm^{-1})
pH	4.7	5.1
Eh	664 (mV)	639 (mV)
Al (OES)	11725	19731
Ba (MS)	56	26
Ca (OES)	445000	289200
Cd (MS)	43	33
Co (MS)	1380	1166
Cu (MS)	37	145
Fe (MS)	491	67
K (OES)	7900	3560
Li (MS)	215	184
Mg (OES)	684990	344000
Mn (OES)	69800	49400
Na (OES)	22000	5670
Ni (MS)	7679	6330
Si (OES)	19410	16930
Sr (OES)	905	514
Zn (OES)	1813	1305
Fluoride (IC)	4400	6840
Chloride (IC)	156200	33200
Sulfate (IC)	3916000	2222000
Nitrate (IC)	5100	< 2

Table 3: Electrical conductivity, pH and total carbon content in the different layers of soil profiles P1 and P2.

Profile		Total Carbon (g kg^{-1})	EC (µScm^{-1})	pH
P1	15	0.54 ± 0.2	188 ± 5	4.1 ± 0.2
	30	0.41 ± 0.1	163 ± 2	4.0 ± 0.0
	50	0.69 ± 0.0	244 ± 10	3.9 ± 0.1
	65	1.06 ± 0.2	905 ± 54	4.6 ± 0.1
	75	0.24 ± 0.1	1360 ± 17	4.1 ± 0.4
	80	0.51 ± 0.0	772 ± 26	5.6 ± 0.1
	90	0.28 ± 0.2	658 ± 10	4.7 ± 0.2
	95	0.26 ± 0.1	495 ± 2	4.7 ± 0.0
	105	0.59 ± 0.0	818 ± 14	4.7 ± 0.1
P2	20	1.74 ± 0.3	930 ± 24	4.3 ± 0.1
	50	0.20 ± 0.1	764 ± 18	5.1 ± 0.0
	60	0.20 ± 0.1	370 ± 7	5.1 ± 0.2
	65	0.36 ± 0.1	755 ± 30	5.0 ± 0.1
	75	0.33 ± 0.1	725 ± 29	4.3 ± 0.1
	90	0.44 ± 0.0	1045 ± 20	4.0 ± 0.1

Table 4: Chemical composition of polished thin sections prepared from the Mn oxide barrier layers in soil profiles P1 and P2, in weight percentage of major and minor elements from spot analyses (limit of detection = 0.1 wt %). The associated images and exact location of the analysed spots are shown in Fig. 4.

	SiO_2	Al_2O_3	MnO	FeO	BaO	NiO	CaO
Image1							
Point A	< 0.1	0.55	87.37	< 0.1	4.81	1.15	1.79
Point B	5.65	5.56	< 0.1	86.76	< 0.1	< 0.1	< 0.1
Point Q	85.14	10.23	0.55	< 0.1	< 0.1	< 0.1	< 0.1
Image2							
Point A	< 0.1	1.45	89.88	< 0.1	7.89	2.40	1.24
Point Q	79.44	5.67	0.88	10.3	< 0.1	< 0.1	< 0.1
Image3							
Point A	< 0.1	0.40	82.09	< 0.1	15.95	< 0.1	1.15
Point B	3.91	< 0.1	< 0.1	93.41	< 0.1	< 0.1	< 0.1
Image4							
Point A	0.38	0.79	81.98	< 0.1	14.55	< 0.1	1.57

Table 5: Sequence similarity of isolated Mn(II)-oxidizing bacteria identified from the Mn oxide barrier layers in soil profiles P1 and P2.

	Strains	Accession number	Closest similarity	Accession number	Sequence identity (%)
1	GH_P2_28	JX999616	Bacillus safensis	NR_113945	98
2	GH_P2_27	JX999618	Brevibacillus reuszeri	NR_113802	98
3	GW_P6_24	JX999617	Bacillus altitudinis	NR_042337	99
4	GH_P2_3	JX999613	Arthrobacter stackebrandtii	NR_042258	97
5	GH_P2_6	JX999614	Frondihabitans australicus	NR_043897	96
6	GH_P4_8	JX999615	Sphingomonas mucosissima	NR_042493	94